Int. J. Multiphase Flow Vol. 14, No. 3, pp. 321–331, 1988
Printed in Great Britain.

0301-9322/88 $3.00 + 0.00

ANALYSIS OF AN ANNULAR–MIST FLOW MODEL IN A T-JUNCTION

E. ŚLIWICKI and J. MIKIELEWICZ
Institute of Fluid Flow Machinery, Polish Academy of Science, 80-952 Gdańsk, Poland

(*Received* 20 *September* 1985; *in revised form* 2 *November* 1987)

Abstract—Gas–liquid two-phase flow in a T-junction with a horizontal side tube was analysed. Gravity effects were neglected. An annular–mist flow pattern was assumed at the inlet to the T-junction. Based on the simple models of film- and gas–droplet core flow the relations for the liquid mass flowrate in the side tube, as a function of the gas flowrate, were derived. The results of the calculations were compared with previous experimental data.

1. INTRODUCTION

During the design process it is often necessary to determine the two-phase gas–liquid flow distribution in a variety of pipe systems which include T-junctions.

Often the problem lies in obtaining equal flowrate distributions for both phases. However, the problem usually remains unsolved, resulting in the flowrate ratio of both phases in the outlet pipe of the T-junction being different from that in the inlet pipe.

The problems described above are found in certain types of process plant and water-cooled nuclear reactors.

Despite the fact that the problem is important there are few experimental results and theoretical investigations reported in the literature; one such analytical flow model was proposed by Saba & Lahey (1984).

The following analysis presents a simple model of the annular–mist two-phase flow distribution in a T-junction. In annular–mist flow, the liquid phase flows as a thin annular film on the inner wall of the tube and as drops entrained into the gas core, flowing along the centre of the channel.

The analysis concerns a T-junction with a horizontal side tube; gravitational force was neglected. The position of the main tube was not pre-determined on the grounds that the annular–mist flow structure does occur within it.

The results of the calculations performed on the basis of the proposed model were compared with the experimental data of Azzopardi & Whalley (1982)—AERE Harwell, where the majority of work concerning this problem was performed. It seems that with regard to design calculation practice, the agreement of the results is quite acceptable.

2. MODEL OF TWO-PHASE FLOW IN A T-JUNCTION

Let us consider two-phase flow in a T-junction (figure 1) with horizontal side pipe 1. The inlet and outlet cross-section areas of the main pipe are equal $A_3 = A_2$.

At the inlet (3) to the T-junction it is assumed that the flow structure is of annular–mist type, with liquid film flowrate $\dot{m}_{f3}$, gas core flowrate $\dot{m}_{G3}$ and (uniformly distributed throughout the gas core) liquid droplet flowrate $\dot{m}_{d3}$.

The objective of the analysis is to determine the total liquid flowrate $\dot{m}_{L1}$ in the side pipe as a function of the gas flowrate $\dot{m}_{G1}$. The side flowrate $\dot{m}_{L1}$ comprises part of the main film flowrate $\dot{m}_{f3}$ which enters side pipe 1, $\dot{m}_{f1}$, and the droplet flowrate $\dot{m}_{d1}$.

The gas and liquid flowrates in side pipe 1 are usually related to the inlet gas flowrate $\dot{m}_{G3}$ and the total liquid flowrate $\dot{m}_{L3}$.

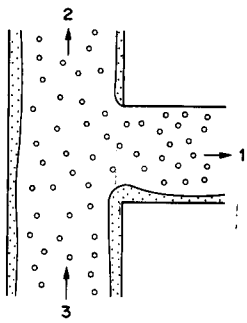

Figure 1. Schematic view of two-phase flow in a T-junction.

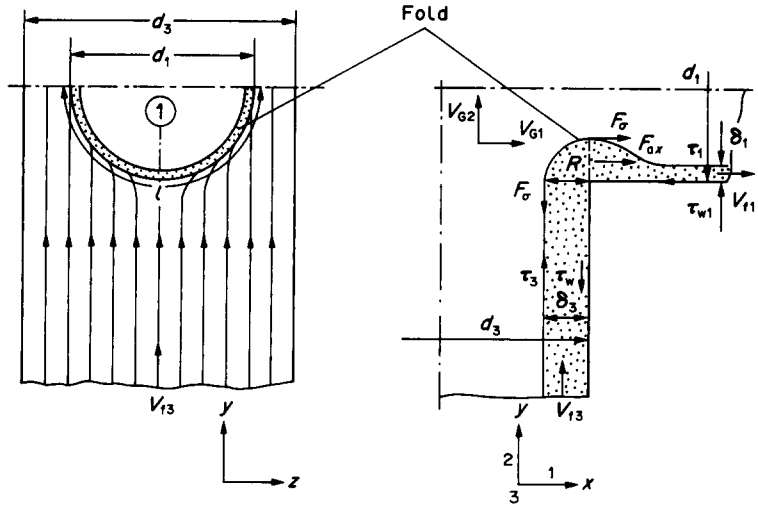

Figure 2. Liquid film flow in a T-junction.

In order to facilitate a comparison of the results with the experimental data of Azzopardi & Whalley (1982), we relate the liquid flowrate $\dot{m}_{L1}$ to the inlet film flowrate $\dot{m}_{f3}$,

$$m^*_{L1} \triangleq \frac{\dot{m}_{L1}}{\dot{m}_{f3}} = \frac{\dot{m}_{f1} + \dot{m}_{d1}}{\dot{m}_{f3}} = m^*_{f1} + \tilde{m}_{d1} m^*_{G3} \qquad [1]$$

where

$$m^*_{f1} \triangleq \frac{\dot{m}_{f1}}{\dot{m}_{f3}},$$

$$m^*_{G3} \triangleq \frac{\dot{m}_{G3}}{\dot{m}_{f3}}$$

and

$$\tilde{m}_{d1} \triangleq \frac{\dot{m}_{d1}}{\dot{m}_{G3}};$$

or, by introduction of the relative flowrate of droplets extracted in side pipe 1,

$$k \triangleq \frac{\tilde{m}_{d1}}{\tilde{m}_{d3}} \qquad [2]$$

where

$$\tilde{m}_{d3} \triangleq \frac{\dot{m}_{d3}}{\dot{m}_{G3}},$$

the liquid flow balance in pipe 1 can be written as

$$m^*_{L1} = m^*_{f1} + k\tilde{m}_{d3} m^*_{G3}. \qquad [3]$$

In order to determine the total side liquid flowrate m^*_{L1}, assuming that the inlet flowrates m^*_{G3} and $\tilde{m}_{d3}$ are known, it is necessary to determine the side film flowrate m^*_{f1} and k. These quantities will be determined later in the analysis.

2.1. Film flowrate m^*_{f1}

The liquid film flow in a T-junction is shown schematically in figure 2. A uniform liquid film of mass flowrate $\dot{m}_{f3}$ and thickness δ_3 flows in pipe 3 in the y-direction with mean velocity V_{f3}.

Let us consider a strip of the film of width $l = \pi d_1/2$ and flowrate $\dot{m}'_{f3}$. On reaching the junction, it forms an arc fold of width l and mean radius of curvature R. The fold is three-dimensional and

hence two additional curvatures of radii $d_1/2$ and $d_3/2$ should be considered. However, they are much greater than R and therefore can be neglected.

Surface tension forces acting on the fold in the x- and y-directions are equal and can be written as

$$F_\sigma = \sigma_{d_1}. \tag{4}$$

The strip stream $\dot{m}'_{f3}$ slows to zero, owing to the surface tension force in the y-direction. Part of the stream then flows along the perimeter of the hole of side pipe inlet 1 (see figure 2) and enters outlet pipe 2; the rest, owing to the surface tension force F_σ and the drag force F_a, enters side pipe 1. It is also assumed that the shear stress τ on the gas–liquid interface is approximately equal to the shear stress τ_w on the wall.

Owing to the surface tension force F_σ, a liquid flowrate $\dot{m}^0_{f1}$—called the zero film flowrate—creeps into side pipe 1 even if no gas flow occurs in the side pipe ($\dot{m}_{G1} = 0$). It carries momentum $\dot{m}^0_{f1} V^0_{f1}$.

Due to the drag force F_a, the gas stream drives part of the fold downstream into the side pipe and gives it momentum $\dot{m}^G_{f1} V^G_{f1}$. On neglecting the influence of the static pressure difference, the equation of momentum along the x-coordinate can be written as

$$F_\sigma + F_{ax} = \dot{m}^0_{f1} V^0_{f1} + \dot{m}^G_{f1} V^G_{f1}. \tag{5}$$

The drag force along x-coordinate is

$$F_{ax} = \mathrm{b} R d_1 V^2_{G1}, \tag{6}$$

where b is a constant and V_{G1} is the cross-section mean velocity. With the use of the relation

$$\frac{\dot{m}_{G1}}{\dot{m}_{G3}} = \frac{V_{G1} A_1}{V_{G3} A_3}, \tag{7}$$

the velocity V_{G1} can be expressed in terms of non-dimensional quantities:

$$V_{G1} = V_{G3} \frac{\tilde{m}_{G1}}{\aleph}, \tag{8}$$

where

$$\tilde{m}_{G1} \triangleq \frac{\dot{m}_{G1}}{\dot{m}_{G3}},$$

$$\aleph \triangleq \frac{A_1}{A_3}.$$

On the assumption that the radius of curvature of the fold $R \approx \text{const}$ and is independent of the gas flowrate $\tilde{m}_{G1}$, and taking [8] into account, the drag force in [6] can be expressed in terms of non-dimensional quantities:

$$F_{ax} = \mathrm{b}_1 \frac{\tilde{m}^2_{G1}}{\aleph^{3/2}}, \tag{9}$$

where

$$\mathrm{b}_1 = \text{const} = \mathrm{b} R d_3 V^2_{G3}.$$

The assumption that the radius of curvature of the fold $R = \text{const}$ seems to be quite reasonable, because on reaching the junction only part of the inlet stream is extracted into the side pipe; the rest flows along the edge of the hole and enters pipe 2. The shape of the fold remains constant because film flowrate $\dot{m}'_{f3} > \dot{m}^G_{f1}$; this shape is supposed to change for large gas flowrates ($\tilde{m}_{G1} \to 1$) and in this range the model may diverge from reality.

By introducing [9] and [4] into [5] and dividing by $\dot{m}_{f3} V_{f3}$, one obtains

$$\frac{\sigma d_3}{\dot{m}_{f3} V_{f3}} \sqrt{\aleph} + \mathrm{b}_2 \frac{\tilde{m}^2_{G1}}{\aleph^{3/2}} = m^{*G}_{f1} \frac{V^G_{f1}}{V_{f3}} + m^{*0}_{f1} \frac{V^0_{f1}}{V_{f3}}, \tag{10}$$

where

$$b_2 = \frac{b_l}{\dot{m}_{f3} V_{f3}}.$$

Assuming that the width of the film strip at the point where its velocity equals V_{fl} is the same as at the inlet to side pipe 1, $=l$, the following relation can be written:

$$\frac{\dot{m}_{fl}^G}{\dot{m}_{f3}} = \frac{V_{fl}^G}{V_{f3}} \frac{l\delta_1}{\pi d_3 \delta_3}, \tag{11}$$

where δ_1 is the liquid film thickness in the side pipe at the point where the film velocity is V_{fl}^G.

For a linear velocity profile the mean velocity of shear stress driven liquid film under hydrodynamic equilibrium equals

$$V_{fl} = \frac{\tau\delta}{2\mu}. \tag{12}$$

Hence the ratio of side pipe 1 liquid film thickness to main pipe 3 liquid film thickness can be written as follows:

$$\frac{\delta_1}{\delta_3} = \frac{V_{fl}^G}{V_{f3}\left(\frac{\tau_1}{\tau_3}\right)} \tag{13}$$

and because

$$\frac{\tau_1}{\tau_3} \approx \left(\frac{V_{G1}}{V_{G3}}\right)^2, \tag{14}$$

then

$$\frac{\delta_1}{\delta_3} = \frac{V_{fl}^G}{V_{f3}\left(\frac{V_{G1}}{V_{G3}}\right)^2}. \tag{15}$$

By substituting [15] into [11] and by utilizing the result in [10], the latter takes the following form:

$$\frac{\sigma d_3}{\dot{m}_{f3} V_{f3}} \sqrt{\aleph} + b_2 \frac{\tilde{m}_{G1}^2}{\aleph^{3/2}} = \frac{\sqrt{2}(m_{fl}^* - m_{fl}^{*0})^{3/2}}{\aleph^{5/4}} \tilde{m}_{G1} + m_{fl}^{*0} \frac{V_{fl}^0}{V_{f3}}. \tag{16}$$

The above equation should remain valid for the two extreme cases:

$$\tilde{m}_{G1} = 0, \quad m_{fl}^* = m_{fl}^{*0};$$
$$\tilde{m}_{G1} = 1, \quad m_{fl}^* = 1. \tag{17}$$

The first condition yields

$$\frac{d_3\sigma}{\dot{m}_{f3} V_{f3}} \sqrt{\aleph} = m_{fl}^{*0} \frac{V_{fl}^0}{V_{f3}}; \tag{18}$$

and the second,

$$b_2 = \sqrt{2}\aleph^{1/4}(1 - m_{fl}^{*0})^{3/2}. \tag{19}$$

By substituting [18] and [19] into [16], the final equation is obtained:

$$m_{fl}^* = m_{fl}^{*0} + (1 - m_{fl}^{*0})\tilde{m}_{G1}^{2/3}. \tag{20}$$

The variation of the non-dimensional film flowrate m_{fl}^* with the non-dimensional gas flowrate $\tilde{m}_{G1}$ in the side pipe, for three different coefficients of cross-section area change $\aleph$, are shown in figure 3.

The relative zero film flowrate m_{fl}^{*0} for no gas flow in the side pipe is presented below. The dashed line in figure 3 illustrates the case of the ideal phase distribution, for which the ratio of gas flowrate to total flowrate in the side pipe is the same as at the inlet.

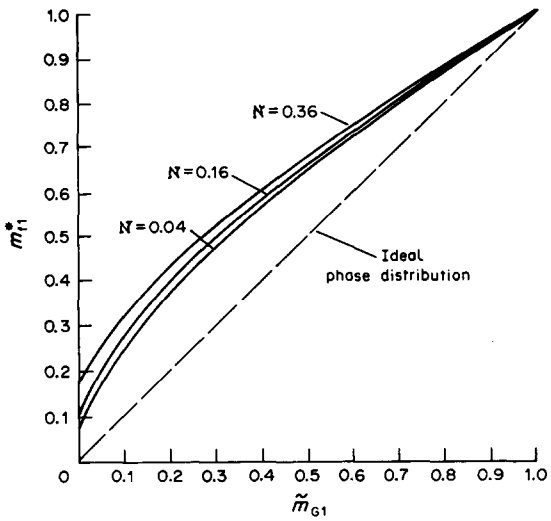

Figure 3. Variation of the film flowrate m^*_{f1} with the gas flowrate $\tilde{m}_{G1}$.

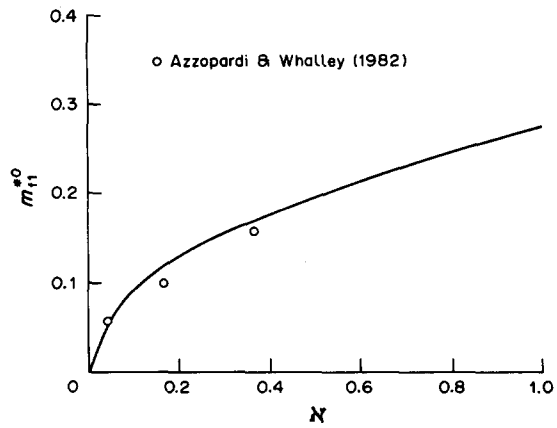

Figure 4. Variation of the zero film flowrate m^{*0}_{f1} with the coefficient of cross-section area change $\aleph$.

2.2. *Zero film flowrate* m^{*0}_{f1}

It is assumed that the film flow $\dot{m}'_{f3}$ of a strip of width l is slowed to zero by the surface tension force F_σ along the y-coordinate (figure 2). The second assumption is that the velocity reduces to zero in a very short distance and hence the differences in static pressure along this distance can be neglected and the shear stresses on both two-phase interfaces can be assumed equal, $\tau_3 = \tau_w$.

In view of these assumptions, the momentum balance for the stream $\dot{m}'_{f3}$ takes the following form:

$$F_\sigma = \dot{m}'_{f3} V_{f3} \qquad [21]$$

and because (see figure 2)

$$\frac{m'_{f3}}{\dot{m}_{f3}} = \frac{l}{\pi d_3} = \frac{\sqrt{\aleph}}{2} \qquad [22]$$

and

$$V_{f3} = \frac{\dot{m}_{f3}}{\rho_L \delta_3 \pi d_3} \qquad [23]$$

then, by utilizing [4], [21] takes the following form:

$$\frac{\dot{m}^2_{f3}}{\rho_L \delta_3 \pi d_3} = \frac{2\sigma d_1}{\sqrt{\aleph}}. \qquad [24]$$

With the assumption that there is no gas flow in the x-direction, the movement of the zero film flowrate $\dot{m}^0_{f1}$ appears to be due to surface tension force F_σ only.

If friction on the two-phase interfaces is neglected, the momentum equation in this direction takes the form

$$F_\sigma = \dot{m}^0_{f1} V^0_{f1}. \qquad [25]$$

If, additionally, no energy losses over the velocity stabilizing distance (to V^0_{f1}) are assumed, the equation of mechanical energy for the film "forced out" into the side pipe simplifies to

$$\frac{\rho_L V^{02}_{f1}}{2} = \frac{\sigma}{R} + \rho_L g \Delta h, \qquad [26]$$

where Δh, in potential energy terms, is the difference between the fold height R at the inlet to the side arm and the film thickness at the velocity stabilizing distance.

From [25] and [26] one can derive the relation for the relative zero film flow "forced out" into the side pipe:

$$m_{\mathrm{fl}}^{*0} = 0.5\sqrt{\frac{\aleph\sigma}{\pi\delta_3\left(\frac{\sigma}{R}+\rho_{\mathrm{L}}g\Delta h\right)}}. \qquad [27]$$

In order to calculate this flowrate, one must know the dimensions of the forming fold and the film thickness at the inlet to the junction and in the side arm.

With the assumption that $R \approx \delta_3$, the potential energy term becomes sufficiently small compared to the surface tension term. By neglecting the first term the following simplified relation is obtained:

$$m_{\mathrm{fl}}^{*0} \approx 0.5\sqrt{\frac{\aleph}{\pi}}. \qquad [28]$$

A graphic interpretation of equation [28] is presented in figure 4. Experimental points from Azzopardi & Whalley (1982) are included in the diagram.

2.3. Droplet relative flowrate k

The gas velocity at the junction has two components: V_{G1} in the x-direction and V_{G2} in the y-direction. The liquid phase $\dot{m}_{\mathrm{d3}}$ (uniformly distributed in the gas core $\dot{m}_{\mathrm{G3}}$) moves downstream with gas velocity V_{G3} (no slip is assumed). A schematic view of the droplet trajectory is shown in figure 5a. A drop passing through inlet cross-section AB, on which the origin of the coordinates was set, has velocity V_{G3}. Immediately afterwards it accelerates in the x-direction due to the drag force of the gas stream entering the side pipe, $\dot{m}_{\mathrm{G1}}$. The origin of the coordinates was set at such a point on the inlet cross-section AB that all drops from the shaded area in figure 5b flow into the side pipe. The area is a circular sector of rise OB = h and area A_h. Line OC is the boundary path for droplet stream $\dot{m}_{\mathrm{d1}}$.

In the y-direction a droplet decelerates due to the opposite drag force. It is assumed that the force is too small to change the droplet velocity along the distance d_1 and

$$V_{\mathrm{d}y} = V_{\mathrm{G3}}. \qquad [29]$$

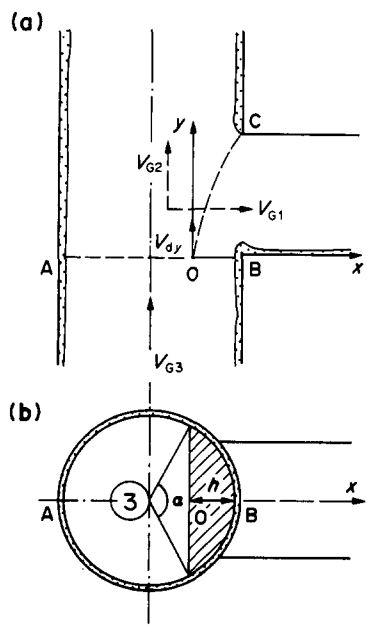

Figure 5. Liquid droplet trajectory in the gas core at a junction.

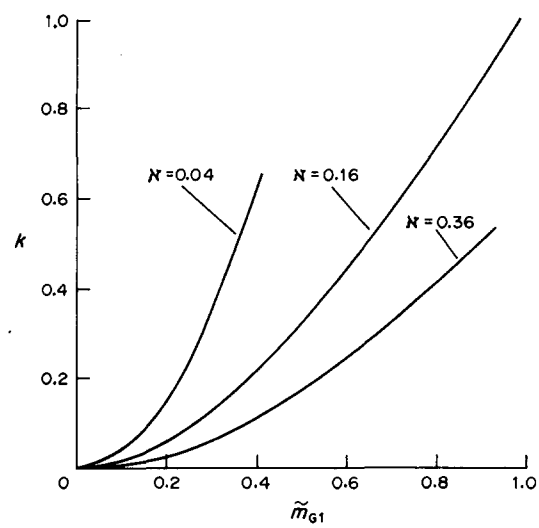

Figure 6. Droplet flowrate k vs gas flowrate $\tilde{m}_{\mathrm{G1}}$.

In the x-direction the droplet velocity rises from zero at the coordinate origin and the equation of motion is as follows:

$$m_d \frac{dV_{dx}}{dt} = C_d A_d \rho_G \frac{(V_{G1} - V_{dx})^2}{2}, \quad [30]$$

where C_d is the drag coefficient for turbulent flow over a spherical droplet of cross-section area A_d and diameter D. For $10 < Re_d < 10^3$, C_d can be approximated by

$$C_d = 24.25(\ln Re_d)^{-2.1}, \quad [31]$$

where the Reynolds number is defined as

$$Re_d = \frac{D\rho_G(V_{G1} - V_{dx})}{\mu_G}. \quad [32]$$

Since $V_{G1} \gg V_{dx}$, then

$$Re_d \approx \frac{D\rho_G V_{G1}}{\mu_G} \quad [33]$$

has been assumed. Actually, the Reynolds number tends to decrease with a rise in the droplet velocity.

By integrating [30] and taking into account that for $t = 0$ the velocity $V_{dx} = 0$, one obtains

$$V_{dx} = \frac{C_1 V_{G1}^2 t}{d_3 + C_1 V_{G1} t}, \quad [34]$$

where

$$C_1 = 0.75 \cdot C_d \frac{\rho_G}{\delta_L} \frac{d_3}{D}.$$

The rise h of the circular segement, see figure 5b, was obtained by integrating

$$h = \int_0^{t_1} V_{dx} dt, \quad [35]$$

where t_1 is the duration of droplet flow over distance d_1 in the y-direction.

After integrating one obtains

$$h = V_{G1} t_1 - \frac{d_3}{C_1} \ln\left(1 + \frac{C_1}{d_3} V_{G1} t_1\right). \quad [36]$$

If time, defined as

$$t_1 = \frac{d_1}{V_{dy}} = \frac{d_1}{V_{G3}}, \quad [37]$$

and [8] are included in [36], one finally obtains

$$\frac{h}{d_3} = \frac{\tilde{m}_{G1}}{\sqrt{\aleph}} - \frac{1}{C_1}\left(1 + C_1 \frac{\tilde{m}_{G1}}{\sqrt{\aleph}}\right). \quad [38]$$

This allows one to calculate the area of the circular segment A_h and, finally, the relative droplet flowrate k if

$$k = \frac{\tilde{m}_{d1}}{\tilde{m}_{d3}} = \frac{A_h}{A_3}. \quad [39]$$

The circular segment area is

$$A_h = 0.5(\alpha - \sin\alpha)\left(\frac{d_3}{2}\right)^2, \quad [40]$$

where the angle α is shown in figure 5b.

Finally, the relation

$$k = \frac{1}{2\pi}(\alpha - \sin\alpha) \qquad [41]$$

was derived, where

$$\alpha = 2\arcsin\left[2\sqrt{\frac{h}{d_3}\left(1-\frac{h}{d_3}\right)}\right] \quad \text{for} \quad 0 < \frac{h}{d_3} < 0.5$$

and

$$\alpha = 2\pi - 2\arcsin\left[2\sqrt{\frac{h}{d_3}\left(1-\frac{h}{d_3}\right)}\right] \quad \text{for} \quad 0.5 \leqslant \frac{h}{d_3} \leqslant 1.$$

Diagrams illustrating k as a function of the non-dimensional gas flowrate $\tilde{m}_{G1}$ for the same values of $\aleph$ as before are shown in figure 6.

3. DISCUSSION OF THE RESULTS

Based on [3], [20], [28], [38] and [41], diagrams of the total non-dimensional liquid flowrate m^*_{L1} and film flowrate m^*_{f1} in the side pipe as a function of the non-dimensional gas flowrate are presented in figures 7–9 for cross-section area change values of $\aleph = 0.04$, 0.16 and 0.36, and for various parameters characteristic of the inlet stream structure.

Plots I, II and III are for $m^*_{G3} = 5.35$ and $\tilde{m}_{d3} = 0.05$ and plots IV, V and VI for $m^*_{G3} = 1.44$ and $\tilde{m}_{d3} = 0.5$. The function $m^*_{L1} = f(\tilde{m}_{G1})$ is approximately linear. This is confirmed by experimental data presented in the literature which are usually approximated by straight lines. The dashed lines in figures 7–9 illustrate the ideal phase distribution, i.e. $X_1 = X_3$. Figure 9 shows the curves (III and VI) calculated for $\aleph = 0.04$. They start from $\tilde{m}_{G1} \geqslant 0.1$ because of the limitations introduced in formula [31]. The same limitations are the reason that the curve of the droplet flowrate k is cut for $\tilde{m}_{G1} \approx 0.4$, as is seen in figure 6. The influence of droplet flow $\tilde{m}_{d1}$ is noticeable in all cases.

As mentioned above, the problem is rather unrecognized and new experimental data is needed for further verification of the model presented here. The only work which included the necessary information and was available to the authors was the report by Azzopardi & Whalley (1982), who

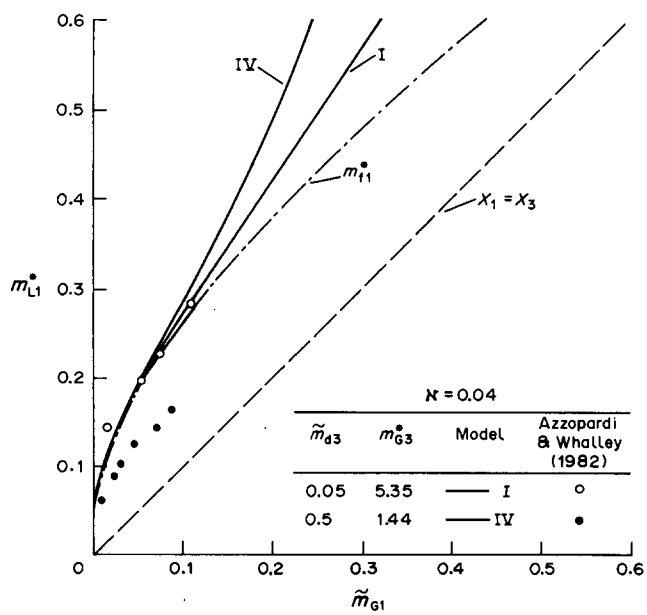

Figure 7. Variation of the liquid flowrate m^*_{L1} with the gas flowrate in the side pipe $\tilde{m}_{G1}$ ($\aleph = 0.04$).

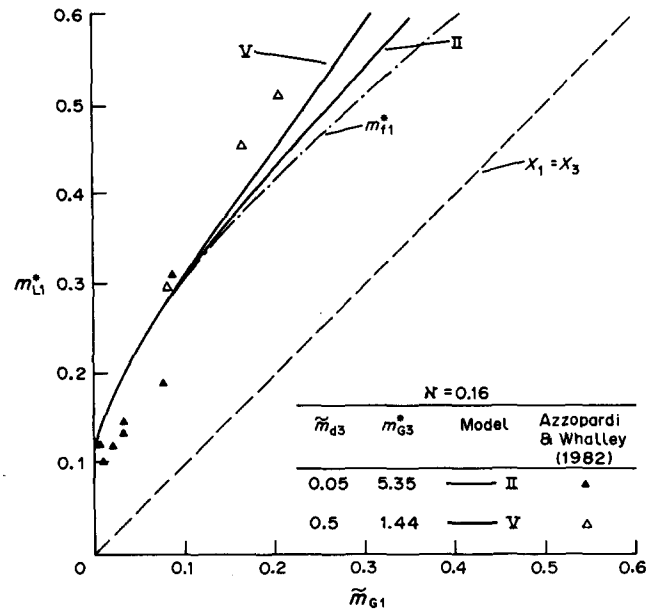

Figure 8. Variation of the liquid flowrate m^*_{L1} with the gas flowrate in the side pipe $\tilde{m}_{G1}$ ($\mathcal{N} = 0.16$).

investigated the distribution of two-phase flow of different flow structures in a vertical T-junction. The present authors used experimental data for annular flow. It is presented in figures 7–9. Theoretical results were calculated for the corresponding inlet conditions $\dot{m}^*_{G3}$ and $\tilde{m}_{d3}$. The agreement of the results is acceptable.

Instead of the function $m^*_{f1} = f(\tilde{m}_{G1})$, the relation of the mass quality X_1 in the side pipe to the mass quality X_3 in the inlet pipe can be derived.

If the above qualities are defined as

$$X_1 \triangleq \frac{\dot{m}_{G1}}{\dot{m}_1} \quad \text{and} \quad X_3 \triangleq \frac{\dot{m}_{G3}}{\dot{m}_3}, \qquad [42]$$

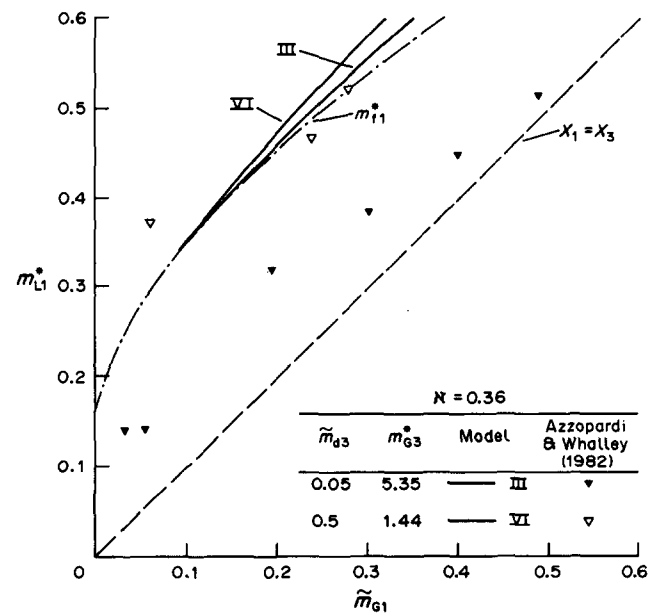

Figure 9. Variation of the liquid flowrate m^*_{L1} with the gas flowrate in the side pipe $\tilde{m}_{G1}$ ($\mathcal{N} = 0.36$).

where

$$\dot{m}_1 = \dot{m}_{G1} + \dot{m}_{f1} + \dot{m}_{d1}$$

and

$$\dot{m}_3 = \dot{m}_{G3} + \dot{m}_{f3} + \dot{m}_{d3},$$

[20] can be rearranged into the following form:

$$\frac{\dfrac{1-X_1}{X_3}\dfrac{\dot{m}_1}{\dot{m}_3}\dfrac{1}{\tilde{m}_{d3}} - k}{\dfrac{1-X_3}{X_3}\dfrac{1}{\tilde{m}_{d3}} - 1} = m_{f1}^{*0} + (1 - m_{f1}^{*0})\left(\frac{X_1}{X_3}\right)^{2/3}\left(\frac{\dot{m}_1}{\dot{m}_3}\right)^{2/3}, \qquad [43]$$

where k is expressed by [41] and m_{f1}^{*0} by [28].

The relation h/d_3, given by [38], is now expressed in terms of new variables:

$$\frac{1}{\sqrt{\aleph}}\frac{X_1}{X_3}\frac{\dot{m}_1}{\dot{m}_3} - \frac{1}{C_1}\ln\left(1 + \frac{C_1}{\sqrt{\aleph}}\frac{X_1}{X_3}\frac{\dot{m}_1}{\dot{m}_3}\right). \qquad [44]$$

The function $X_1 = f(X_3)$ is presented in figure 10 for: three different cross-section area change coefficients, $\aleph = 0.04$, 0.16 and 0.36; for flowrate ratio $\dot{m}_1/\dot{m}_3 = 0.5$; and for non-dimensional droplet flowrate $\tilde{m}_{d3} = 0.05$.

4. CONCLUSIONS

(1) The presented phenomenon is complex even for a single T-junction and annular flow. The proposed theoretrical model is a kind of idealization and should be treated as a proposition of a physically-based approach to the problem. The model is valid for smooth films, whereas in fact the real film is a wavy structure and its geometry and behaviour depend roughly on gas velocity. The model is supposed to be more accurate for lower gas velocities for which the film is smoother.

There may be a case where the results of measurements differ from the theoretical predictions based on the presented equations. This stems from the fact that annular two-phase flow is observed in wide range of flow parameters [see Azzopardi & Whalley (1982), the diagram of $m_{L1}^{*} = f(\tilde{m}_{G1})$].

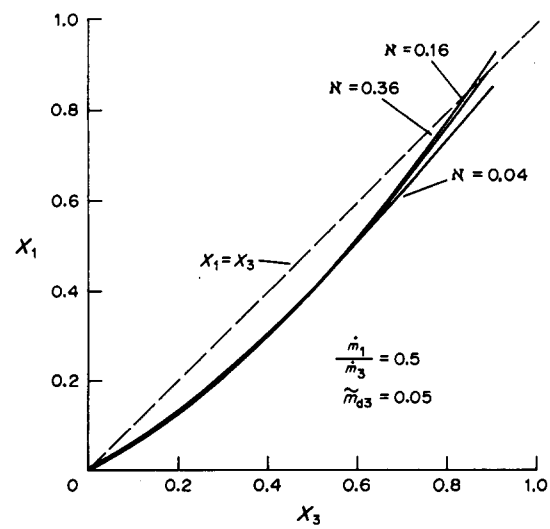

Figure 10. Variation of the side pipe mass quality X_1 with the inlet mass quality X_3 for different coefficients of cross-section area change $\aleph$.

The model is the introductory approach to the analysis of the problem and can be modified by, for example, taking the wavy film interface into account.

The comparison of the theoretical predictions with the experimental results proved the validity of the assumptions of the model.

(2) For greater gas flowrate $\tilde{m}_{G1}$ the function $m^*_{L1} = f(\tilde{m}_{G1})$ is approximately linear, which agrees with the experimental data of other authors.

(3) Inlet parameters, such as m^*_{G3} and $\tilde{m}_{d3}$, influence the droplet flowrate $\tilde{m}_{d1}$ only.

(4) Experimental investigations pointed out the existence of liquid flow in the side pipe if no gas flow occurs there. The analysis proved that this zero film flowrate m^{*0}_{f1} depends only on the coefficient of cross-section area change $\aleph$. This is confirmed by the experimental data of Azzopardi & Whalley (1982) and Azzopardi (1984).

(5) In order to perform a detailed verification of the model, complete evidence of experimental investigations on stabilized annular–mist two-phase flow is necessary.

REFERENCES

AZZOPARDI, B. J. 1984 The effect of the side arm diameter on the two-phase flow split at a T-junction. *Int. J. Multiphase Flow* **10,** 509–512.

AZZOPARDI, B. J. & WHALLEY, P. B. 1982 The effect of flow patterns on two-phase flow in a T-junction. *Int. J. Multiphase Flow* **8,** 491–507.

SABA, N. & LAHEY, R. T. 1984 The analysis of phase separation phenomena in branching conduits. *Int. J. Multiphase Flow* **10,** 1–20.

UEDA, T. & KIM, K. 1982 Dryout heat flux and size of entrained drops in a flow boiling system. *Bull. JSME* **25,** 225–233.